Effect of Turbulence on Wave Propagation in Evaporation Ducts above a Rough Sea Surface

Yung-Hsiang Chou and Jean-Fu Kiang
Graduate Institute of Communication Engineering, National Taiwan University, Taipei, Taiwan
(E-mail: jfkiang@ntu.edu.tw)

***Abstract*—A proper set of models are carefully selected from the literatures to form a wholistic perspective in simulating the wave propagation in evaporation ducts, under a close-to-realistic environment. The split-step Fourier (SSF) propagation algorithm is applied to analyze the propagation properties in evaporation ducts above a rough sea surface, with turbulence in the ducts. The scattering effect of the rough sea surface is modeled with an effective reflection coefficient, including the Miller-Brown correction factor for surface roughness. The turbulence effect is simulated with a two-dimensional Kolmogorov power spectrum of refractive index fluctuation, which is derived from the three-dimensional Kolmogorov power spectrum using the Wiener-Khinchin theorem, including the anisotropic effect of the outer scales. The average M-profile, the outer scales of turbulence, and the structure constant of the refractive index are categorized under different atmospheric conditions. Simulation results are presented and discussed over all possible atmospheric conditions to better understand the effect of turbulence on the evaporation ducts.**

***Index Terms*—Propagation, split-step Fourier (SSF) algorithm, evaporation duct, rough surface, turbulence, Kolmogorov power spectrum, refractive index fluctuation.**

I. Introduction

Measurement of centimeter-wave propagation indicates that the difference between the field values inside and above an evaporation duct is much smaller than the prediction using a simple model [1]. Such difference may be explained as follows [1], [2]: (1) The height and strength of an evaporation duct can vary with distance, and the wave within an irregular duct is less focused. (2) Roughness of sea surface redirects a large portion of wave energy into the space above the duct. (3) Turbulent fluctuations in the atmosphere tends to broaden the angular spectrum of waves and increase leakage from the duct. Scattering by turbulent atmospheric fluctuations is the strongest mechanism, at least in certain cases.

For surface-based radars, non-standard tropospheric refraction such as ducting may result in an anomalous propagation condition, bending the radar ray from the anticipated direction [3]. Anomalous propagation echoes have been observed in fair weather conditions; more frequently in summer than in winter, more frequently in tropical areas than in the middle and higher latitudes [4].

Ducting may seriously affect radio communications links, extend the radar range of a target at or near the sea surface to be considerably longer than if in the free-space [5]. Evaporation duct is a surface duct appearing over water bodies, featuring rapid decrease of humidity with height. It is the most common type of anomalous propagation over oceans and other large bodies of water. The worldwide mean of the evaporation duct height (EDH) is about 10 m [6], sometimes reaches 30 m or 40 m [7]. The EDH increases during the summer months and during the daytime [8]. With the evaporation ducts so close to the sea surface, the latter has very strong effects on the signal propagating in the ducts.

The effects of duct on communications links have been studied [9], [10]. Possible effects of tropospheric ducting on short-distance wireless communications have also been reported [11]. The effects of evaporation and surface-based ducts on microwave path loss have been studied [12]. In [13], the path-loss variations are compared with the monthly and seasonal mean parameters of surface ducts, based on a two-year statistical study of surface-duct formation at Istanbul, over a WCDMA-FDD downlink band [14]. Ducts frequently appear in the coastal areas where the horizontal change of refractivity can not be neglected. In [12], a comparison is made between a range independent surface-based duct and a mixed land-sea path, using two M-profiles.

Propagation experiments have been conducted in the Mediterranean and the North Sea areas [15], [16]. The received signal is stronger than expected, which is a sign that the evaporation ducting effect may dominate over the gaseous absorption in the 10-20 GHz band. Measurements at 18 GHz have been conducted to demonstrate the enhancement on radar coverage and range detection due to an evaporation duct [17], [7]. While the predictions and the measurements seem to agree reasonably well, the predictions tend to underestimate the path loss when the duct heights are low. Although the prediction model incorporates the Kirchhoff theory to account for the scattering from a rough sea surface, it does not consider the scattering due to the turbulent fluctuations in the refractive index [18].

An evaporation duct can significantly increase the signal strength near the sea surface for over-the-horizon paths, at frequencies above 3 GHz. As the frequency is higher than 10 GHz, the signal strength is reduced by scattering from the wind-driven rough sea surface. Such signal reduction is more obvious under strong ducting conditions and large sea-wave heights [19]. In [19], an MLAYER propagation model, including the Miller-Brown reflection reduction factor (RRF), is used to compare with the measurements. In all the

This work was sponsored by the National Science Council, Taiwan, ROC, under contract NSC 100-2221-E-002-232.

cases studied in [19], the model including rough sea surface provides a closer match with the measurement results than the model with smooth sea surface, but the former model still underestimates the path loss by 3 to 12 dB. The refractive-index fluctuation may partly account for this underestimate.

The effects of air turbulence have been analyzed by applying a small-perturbation method to a mode-based model [18], or applying a phase-screen method to a split-step Fourier (SSF) model [20], [21]. Different models have been compared on a series of over-water measurements, in a nearly standard atmosphere [21]. The model including the turbulence scattering performs better than the other models, in the sense of matching with the measured data. At higher frequencies, the effects of turbulent scattering become even stronger.

In [22], two approaches are proposed to model the surface-layer turbulence effects in a marine environment at microwave frequencies. One is the SSF method with phase screen, the other is a direct computation of the log-amplitude variance of signals. Their results are compared with the observation, and the effect of the power-law constant on the first approach is also discussed.

In [23], the phase screen method is adopted in the split-step Fourier algorithm to simulate the turbulence effect in an evaporation duct. It is assumed that the atmosphere is under the neutral condition, the turbulence follows the one-dimensional Kolmogorov spectrum, the structure constant and the outer scale are constant, and the sea surface is smooth [23]. The simulation results show that the refractive-index fluctuation leads to energy leakage away from the duct, causing an additional path loss within the duct. The height distribution of radiated power becomes more uniform than that without the fluctuations. The power leakage along the evaporation duct is not uniform. It is also observed that the received power level above the duct fluctuates more significantly than within the duct when the refractive-index fluctuation is considered.

Diffraction by a relatively smooth sea surface can be described by introducing an effective reflection coefficient [24] into the boundary condition, which is the flat-surface Fresnel reflection coefficient multiplied by a roughness reduction factor (RRF). In general, a rough sea surface tends to destroy the trapping property of the duct structure and changes the path-loss pattern. In [25], the effects of wind direction on electromagnetic waves propagation over rough sea surface are studied by mixing two approaches applicable at large and small roughness, respectively.

The interaction among sea waves is nonlinear, rendering the sea-surface statistics different from a Gaussian distribution [26]. It has been demonstrated that the shadowing effect prevails over the non-Gaussian statistics of a sea surface, especially in the presence of an evaporation duct at the centimeter wavelength [27].

The wave equation can be reduced to a parabolic equation (PE), which is then solved using numerical techniques like the split-step Fourier (SSF) algorithm [28], finite difference (FD) algorithm [24], and finite element (FE) algorithm [29]. The FD and FE algorithms are more flexible to implement various boundary conditions. The SSF algorithm is numerically stable and allows a larger step size to compute the field distribution at long distances.

Reasonable agreement between measured and predicted field strength using the PE model has been achieved in a tropical maritime environment [30]. It is shown that the PE model gives a good estimation of path factor over a wide range of frequencies (X, Ka and W bands) and a variety of atmospheric conditions [31]. The difficulties in predicting the field strength of maritime links and the importance of higher M-inversion can be found in [32].

Numerical analysis indicates that the microwave inside an evaporation duct suffers an additional path loss in the presence of turbulence [33]. Monte-Carlo method has been used to study the scattering properties of scalar waves in randomly fluctuating slabs with an exponential spatial correlation, and it has also been extended to random media with non-exponential spatial correlation and background inhomogeneity [34], [35].

The prediction accuracy of the PE models is constrained by the environmental parameters, especially in littoral environments [12], [36]. Three-dimensional PE models have been developed [37], [38], covering the sea-surface roughness effect [25] and the evaporation ducts [39]. PE-based time-dependent propagation model has also been explored [40].

Although many of the key factors on evaporation ducts, like refractive-index profile, rough surface, wind profile, turbulence, have been analyzed or modeled; few literatures, if not none, integrate all the relevant factors together to analyze or simulate wave propagation in evaporation ducts under a close-to-realistic environment. In this work, we carefully review many existing models about these factors, and choose a proper set of models to simulate the wave propagation in evaporation ducts, under all possible atmospheric conditions. During the review process, it is observed that the wind profile, which can be categorized with a stability index of the atmosphere, seems to be a common factor behind all these models. As a result, this work provides a wholistic perspective on the subject issues. The simulation results may also help reveal more values of the existing models and inspire more ideas from the readers.

In this work, the SSF algorithm is used to simulate wave propagation over long distances. The Miller-Brown [42] formula of RRF is adopted to model the rough sea surface. Monte-Carlo method is used to generate profiles of refractive-index fluctuations to simulate the turbulence in the atmosphere. The relevant models are described in Section II, the proper ranges of parameters in these models are estimated in Section III, the simulation of practical evaporation ducts is presented and discussed in Section IV, followed by the conclusion.

II. Construction of Models

A. Propagation Model

The parabolic equation is a paraxial approximation to the Helmholtz wave equation, under the assumption that the electromagnetic wave predominantly propagates in the horizontal direction, $\hat{x}$. The two-dimensional narrow-angle forward-scattering scalar form of the parabolic equation takes the form [28]

$$\frac{\partial u(x,z)}{\partial x} \simeq -j\left\{\frac{k}{2}[m^2(x,z)-1]+\frac{1}{2k}\frac{\partial^2}{\partial z^2}\right\}u(x,z) \quad (1)$$

where k is the wavenumber in the background medium, $m = 1+M\times10^{-6}$, with the modified refractivity, M, related to the refractivity, N, as $M = N+0.157z$. Eqn. (1) is very accurate with the propagation angle about the horizontal direction falls within $|\theta| < 15^\circ$ [24].

The split-step solution to (1) can be expressed as [28]

$$u(x+\Delta x,z) = e^{-j(k/2)(m^2-1)\Delta x} \mathcal{F}^{-1}\left\{e^{j(p^2/2k)\Delta x}\mathcal{F}\{u(x,z)\}\right\} \quad (2)$$

where $p = k\sin\theta$ is the vertical wavenumber. The solution $u(x,z)$ and its spectrum $U(x,p)$ are related by the Fourier transform $\mathcal{F}\{\cdot\}$ and its inverse $\mathcal{F}^{-1}\{\cdot\}$ as

$$\mathcal{F}\{u(x,z)\} = \frac{1}{\sqrt{2\pi}}\int_{-\infty}^{\infty} u(x,z)e^{jpz}dz$$
$$\mathcal{F}^{-1}\{U(x,p)\} = \frac{1}{\sqrt{2\pi}}\int_{-\infty}^{\infty} U(x,p)e^{-jpz}dp$$

To represent wave propagation over a perfect electric conductor (PEC) surface, either a Dirichlet (horizontal polarization) or a Neumann (vertical polarization) boundary condition is imposed. To represent wave propagation over a smooth impedance surface, the boundary condition can be specified as [43]

$$\left(\frac{\partial}{\partial z} + \alpha_{h,v}\right)u(x,z) = 0 \quad (3)$$

with

$$\alpha_{h,v} = -jk\sin\chi\frac{1-R_{\text{eff}}}{1+R_{\text{eff}}} \quad (4)$$

where $\chi = 90^\circ - \theta_i$ is the grazing angle, R_{eff} is the Fresnel's reflection coefficient, R_F^h or R_F^v, with

$$R_F^h = \frac{\sin\chi - \sqrt{\epsilon_{sr}-\cos^2\chi}}{\sin\chi + \sqrt{\epsilon_{sr}-\cos^2\chi}} \quad (5)$$

$$R_F^v = \frac{\epsilon_{sr}\sin\chi - \sqrt{\epsilon_{sr}-\cos^2\chi}}{\epsilon_{sr}\sin\chi + \sqrt{\epsilon_{sr}-\cos^2\chi}} \quad (6)$$

for the horizontal and the vertical polarization, respectively;

$$\epsilon_{sr} = \epsilon_s/\epsilon_0 = \epsilon_r - j60\sigma\lambda$$

is the effective dielectric coefficient of the sea sea surface, σ and ϵ_r are the conductivity and relative permittivity, respectively, of the sea water [44].

The boundary condition can be incorporated into the standard split-step PE approach through the use of mixed Fourier transform [28], [43]. The path loss (PL) is defined as [24]

$$\text{PL} = 20\log\left(\frac{4\pi\sqrt{x}}{\lambda^{3/2}|u(x,z)|}\right),\ \text{dB} \quad (7)$$

where λ is the wavelength of the wave, and x is the propagation range.

B. Effective Reflection Coefficient of Rough Sea Surface

The roughness effect can be incorporated by multiplying the Fresnel's reflection coefficient, R_F, by a roughness reduction factor (RRF), ρ_{MB}, to obtain an effective reflection coefficient [24]

$$R_{\text{eff}} = \rho_{\text{MB}}R_F$$

where

$$\rho_{\text{MB}} = e^{-\gamma^2/2}I_0\left(\gamma^2/2\right) \quad (8)$$

is the Miller-Brown roughness reduction factor [42], $I_0(\alpha)$ is the zeroth-order modified Bessel function of the first kind. The relevant parameters have the form

$$\gamma = 2k\sigma_h\sin\chi$$
$$\sigma_h = 5.1\times10^{-3}U_{10}^2 \quad (9)$$

where σ_h is the standard deviation of the sea wave, k is the wavenumber of the signal, and U_{10} is the reference wind speed at 10 m above the sea level. Note that the RRF in (8) affects the magnitude of the complex Fresnel reflection coefficient, but does not account for the shadowing effect [45] or the geometry of the sea surface [25]. At near grazing incidence, the shadowing effect may have stronger effect on the wave propagation [45].

C. Refractive Index Fluctuation

The total refractive-index is expressed as

$$n(x,z) = \hat{n}(z) + n_f(x,z) \quad (10)$$

where $\hat{n}(z)$ is the average refractive index, which is a function of altitude, and $n_f(x,z)$ is the fluctuation of the refractive-index. The turbulence is approximated as frozen [46] during the period the electromagnetic wave propagates from the transmitting antenna to the receiving one. By applying the Monte-Carlo technique, one sample profile of refractive-index fluctuation, of a two-dimensional turbulence, can be realized as [34], [41]

$$n_f^{(s)}(x,z) = \sum_{p=1}^{\infty}\sum_{q=1}^{\infty} a_{pq}^{(s)}\sin(\zeta_{xp}x+\zeta_{zq}z) + b_{pq}^{(s)}\cos(\zeta_{xp}x+\zeta_{zq}z) \quad (11)$$

where s indicates the sth realization, ζ_{xp} and ζ_{zq} are the pth and qth discretized wavenumber, respectively, a_{pq} and b_{pq} are random numbers with variance σ_{pq}^2, which can be expressed as

$$\sigma_{pq}^2 = 4\Delta\zeta_{xp}\Delta\zeta_{zq}F_n(\zeta_{xp},\zeta_{zq}) \quad (12)$$

where $F_n(\zeta_x,\zeta_z)$ is the two-dimensional power spectral density of the refractive-index fluctuation.

The three-dimensional power spectral density of refractive-index in an isotropic Kolmogorov turbulence is [47]

$$\Phi_n^{\text{K}}(\zeta_x,\zeta_y,\zeta_z) = \frac{0.033C_n^2}{(\zeta_x^2+\zeta_y^2+\zeta_z^2+1/L_0^2)^{11/6}} \quad (13)$$

Where L_0 is the outer scale, and C_n^2 is the structure constant. By the Wiener-Khinchin theorem [48], the two-dimensional

power spectral density, independent of the y coordinate, can be derived as

$$F_n^{\mathrm{K}}(\zeta_x,\zeta_z)=\int_{-\infty}^{\infty}\Phi_n^{\mathrm{K}}(\zeta_x,\zeta_y,\zeta_z)d\zeta_y = \frac{0.0555C_n^2}{(\zeta_x^2+\zeta_z^2+1/L_0^2)^{4/3}} \tag{14}$$

which is an isotropic Kolmogorov turbulence. Next, follow the same approach as in [47] to modify (14) to be a two-dimensional anisotropic Kolmogorov spectrum

$$F_n^{\mathrm{K}}(\zeta_x,\zeta_z)=\frac{0.0555C_n^2(L_{0h}L_{0v})^{4/3}}{(\zeta_x^2L_{0h}^2+\zeta_z^2L_{0v}^2+1)^{4/3}} \tag{15}$$

where L_{0v} and L_{0h} are the outer scales in the vertical and the horizontal directions, respectively.

III. Estimation of Parameters

A. Average Modified Refractivity

The PJ model is adopted to generate profiles of modified refractivity under different atmospheric conditions as [49], [50]

$$M(z)=M(0)+\frac{z}{8}-\begin{cases} z_d\dfrac{\ln\dfrac{4(1+z/z_0)}{\left(1+\sqrt{1-16z/L_{\mathrm{mo}}}\right)^2}}{8/\sqrt{1-16z_d/L_{\mathrm{mo}}}}, \\ z/L_{\mathrm{mo}}\le 0 \\ z_d\dfrac{\ln(1+z/z_0)+5z/L_{\mathrm{mo}}}{8(1+5z_d/L_{\mathrm{mo}})}, \\ z/L_{\mathrm{mo}}\ge 0 \end{cases} \tag{16}$$

where L_{mo} is the Monin-Obukhov length, z_d (in m) is the duct height, and z_0 (in m) is the roughness length of the surface. Typically, z_0 increases with the wind speed, ranging from 10^{-4} m on a calm open sea to 10^{-3} m in coastal areas with off-sea wind [50]. The value of z/L_{mo} is used to categorize the atmospheric condition: Stable if $z/L_{\mathrm{mo}}>0$, unstable if $z/L_{\mathrm{mo}}<0$, and neutral if $z/L_{\mathrm{mo}}=0$.

B. Monin-Obukhov Length

The Monin-Obukhov length is essentially dependent upon the heat flux and the friction velocity, which can be treated as independent of height within the surface layer. The general characteristics of the atmosphere can be categorized in terms of z/L_{mo} as follows [50]: When L_{mo} is negative with very small magnitude (z/L_{mo} becomes negative with large magnitude), the heat convection dominates. When L_{mo} is negative with large magnitude (z/L_{mo} becomes negative with small magnitude), the mechanical turbulence dominates. When $z/L_{\mathrm{mo}}=0$, only mechanical turbulence contributes. When z/L_{mo} is a small positive number, the mechanical turbulence is slightly damped by the temperature stratification. When z/L_{mo} is a large positive number, the mechanical turbulence is severely reduced by the temperature stratification. The number $|z/L_{\mathrm{mo}}|$ describes the relative significance between heat convection and mechanical turbulence during the daytime, and to what extent the stratification suppresses the mechanical turbulence during the night time, respectively.

TABLE I
Parameters derived from measurements [52].

Stability class	L_{mo} (m)	u_* (m/s)	z_0 (m)	z_i (m)	Exp. no.
vu	-73	0.22	6.2×10^{-5}	-	358
u	-139	0.30	11.1×10^{-5}	-	544
nu	-288	0.42	22.0×10^{-5}	-	600
n	-1531	0.40	19.6×10^{-5}	393	314
ns	314	0.23	6.3×10^{-5}	223	18
s	85	0.15	2.9×10^{-5}	150	73
vs	28	0.12	1.9×10^{-5}	122	109

z_i is the height of the boundary layer.

The Monin-Obukhov length can be estimated from the Richardson number, R_i, as [50]

$$z/L_{\mathrm{mo}}=\begin{cases} R_i, & R_i\le 0 \\ R_i/(1-5R_i), & 0\le R_i\le 0.2 \end{cases} \tag{17}$$

The Richardson number R_i in the surface layer can be expressed as [50]

$$R_i=\frac{g}{T}\frac{\gamma_d-\gamma}{(\partial v_h/\partial z)^2}\left(1+\frac{0.07}{B}\right) \tag{18}$$

where g is the gravity acceleration, $\gamma=-\partial T/\partial z$ is the lapse rate of temperature, $\gamma_d=9.8^\circ$ C/km is the dry adiabatic lapse rate, v_h is the mean wind velocity in the horizontal direction, and

$$B=\frac{T_2-T_1+0.01(z_2-z_1)}{2500(q_2-q_1)} \tag{19}$$

is the estimated Bowen ratio [50], with q the specific humidity.

In [51], seven stability conditions are defined and related to the Monin-Obukhov length: $10\le L_{\mathrm{mo}}\le 50$ m for very stable (vs) condition, $50\le L_{\mathrm{mo}}\le 200$ m for stable (s) condition, $200\le L_{\mathrm{mo}}\le 500$ m for near-neutral stable (ns) condition, $|L_{\mathrm{mo}}|\ge 500$ m for neutral (n) condition, $-500\le L_{\mathrm{mo}}\le -200$ m for near-neutral unstable (nu) condition, $-200\le L_{\mathrm{mo}}\le -100$ m for unstable (u) condition, and $-100\le L_{\mathrm{mo}}\le -50$ m for very unstable (vu) condition.

In [52], measurements were conducted in 2006, at site located 18 km from the west coast of Denmark in the North Sea. A set of mean parameters derived from the measurements are summarized in Table I, categorized under different atmospheric stability conditions just mentioned.

C. Outer Scale of Turbulence

For turbulence in the free atmosphere, the outer scale L_0 typically ranges from 10 to 100 m. The isotropic assumption is usually valid for well-developed turbulence far from any boundaries. In a surface layer, which lies in the lowest 10 % of a planetary boundary layer [50], the horizontal outer scale might remain unchanged, but the vertical outer scale is usually reduced, rendering the turbulence no longer locally homogeneous and isotropic in this layer. The turbulence in the surface layer is dominated by the wind-shear. A first-order vertical outer scale in the surface layer can be expressed as [47], [53]

$$L_{0v}=k_a z\phi_m^{-3/2}\phi_\epsilon^{-1/4} \tag{20}$$

where k_a is the von Karman's constant, ϕ_m is the normalized wind shear, and ϕ_ϵ is the normalized turbulent kinetic energy dissipation rate. The von Karman's constant is conventionally taken to be 0.4. Its value measured in the wind tunnel and the atmosphere ranges from 0.35 to 0.43 [50], [54]. The normalized wind shear is defined as [50]

$$\phi_m = \frac{k_a z}{u_*}\frac{\partial u}{\partial z} \tag{21}$$

and the normalized turbulent kinetic energy dissipation rate is defined as [50]

$$\phi_\epsilon = \frac{k_a z}{u_*^3}\epsilon \tag{22}$$

where u is the wind velocity, u_* is the friction velocity, and ϵ is the dissipation rate. The profiles of ϕ_m and ϕ_ϵ under different conditions are [50]

$$\phi_m = \begin{cases} (1-16z/L_{\rm mo})^{-1/4}, & -2 \le z/L_{\rm mo} \le 0 \\ (1-15z/L_{\rm mo})^{-1/3}, & z/L_{\rm mo} < -2 \\ 1+5z/L_{\rm mo}, & z/L_{\rm mo} > 0 \end{cases}$$
$$\phi_\epsilon = \begin{cases} 1-z/L_{\rm mo}, & z/L_{\rm mo} \le 0 \\ \left[1+2.5\left(z/L_{\rm mo}\right)^{0.6}\right]^{3/2}, & z/L_{\rm mo} > 0 \end{cases} \tag{23}$$

The vertical outer scale of the turbulence in a surface layer, under different atmospheric conditions, are derived by substituting (23) into (20):

$$L_{0v} = \begin{cases} \dfrac{k_a z\left(1-z/L_{\rm mo}\right)^{-1/4}}{\left(1-16z/L_{\rm mo}\right)^{3/8}}, & -2 \le z/L_{\rm mo} \le 0 \\ \dfrac{k_a z\left(1-z/L_{\rm mo}\right)^{-1/4}}{\left(1-15z/L_{\rm mo}\right)^{1/2}}, & z/L_{\rm mo} < -2 \\ \dfrac{k_a z(1+5z/L_{\rm mo})^{-3/2}}{\left[1+2.5(z/L_{\rm mo})^{0.6}\right]^{3/8}}, & z/L_{\rm mo} > 0 \end{cases} \tag{24}$$

where $k_a = 0.4$ [47].

D. Anisotropy of Turbulence

Turbulence at large scales is usually anisotropic, with considerably different outer scales in the horizontal and the vertical directions. The anisotropy and the length of the outer scale is dependent upon the atmospheric stability [55], [56]. The anisotropy of the outer scale becomes more obvious with stronger temperature inversion and weaker wind, which correspond to a higher Richardson number and a more stably stratified atmosphere. In such a weather condition with stable air, the mechanical turbulence is strongly damped by stratification, hence the vertical outer scale become much smaller than the horizontal one. In [55], it is also confirmed that if the turbulent energy is mainly generated from mechanical origin, the eddies are small, the outer scale length tends to decrease with increased wind speed, and vice versa, which is much more obvious in the horizontal scales.

The anisotropy has no significant influence on power fluctuation, but the angle-of-arrival [55]. In [50], the ratio of the horizontal to the vertical integral scale (similar to the outer scale) of wind fluctuations has been estimated. It is shown that with an increasing positive Richardson number, a much larger outer scale is expected in the horizontal direction. Under neutral condition ($R_i \simeq 0$), the horizontal and the vertical outer scales are similar. In an unstable air ($R_i < 0$), eddies tend to be vertically elongated. In [56], it is empirically found that $L_{0h}/L_{0v} \simeq (30 \pm 10)R_i$ under stable condition. The wide range of variation might be attributed to the fact that the anisotropy does not solely depend on R_i.

The anisotropy of the turbulence can be related to the stability of atmosphere as [57]

$$a_z = \frac{10\left(1-z/L_{\rm mo}\right)}{0.5-z/L_{\rm mo}}, \qquad z/L_{\rm mo} < 0.5 \tag{25}$$

where $a_z = 4\pi L_{0h}/L_{0v}$ is the decay constant of the vertical coherence of wind components [50], [58]. Eqn. (25) implies

$$L_{0h}/L_{0v} = \frac{10(1-z/L_{\rm mo})}{4\pi(0.5-z/L_{\rm mo})}, \quad z/L_{\rm mo} < 0.5 \tag{26}$$

E. Structure Constant

Turbulence is likely to become strong (structure constant, C_n^2, becomes large) near the earth surface and in the clouds [59]. The magnitude of C_n^2 generally increases with increasing wavelength, because the contribution of moisture to C_n^2 significantly increases with increasing wavelength. The magnitude of C_n^2 in near-millimeter-wave band can be larger than that in the infrared by orders of magnitude. The magnitude of C_n^2 in the visible and the infrared bands near the ground falls in the range from 10^{-16} to 10^{-12} m$^{-2/3}$ [60].

The structure constant of the refractive-index fluctuation in the planetary boundary layer can be expressed as [47], [53]

$$C_n^2 = a^2 L_{0v}^{4/3}\left(\frac{\partial\langle n\rangle}{\partial z}\right)^2 \tag{27}$$

where a^2 lies between 1.5 and 3.5 [47], [50]. Substituting (16) into (27), we have

$$C_n^2 = 2.8 L_{0v}^{4/3}\times 10^{-12} \begin{cases} \left[0.032+\dfrac{z_d\sqrt{1-16z_d/L_{\rm mo}}}{8}\right. \\ \left.\left(\dfrac{16/L_{\rm mo}}{1-16z/L_{\rm mo}+\sqrt{1-16z/L_{\rm mo}}}+\dfrac{1}{z+z_0}\right)\right]^2, \\ \qquad z/L_{\rm mo} \le 0 \\ \left[0.032+\dfrac{z_d\left[5/L_{\rm mo}+1/(z+z_0)\right]}{8(1+5z_d/L_{\rm mo})}\right]^2, \\ \qquad z/L_{\rm mo} \ge 0 \end{cases} \tag{28}$$

where $a^2 = 2.8$ and $k_a = 0.4$ are chosen [47].

In the experiments considered in [61], the moisture fluctuation plays a dominant role, as compared to temperature, in determining the microwave C_n^2; and significantly affects the acoustic and optical C_n^2 values, since the near-surface turbulence leads to relatively large moisture fluctuations. The overland experiment shows a larger diurnal variation, while the

moisture fluctuation does not play a dominant role [61]. The temperature makes a comparable contribution to microwave C_n^2 near the surface, particularly in the afternoon. For the acoustic and optical waves, the C_n^2 primarily depends on the temperature fluctuations.

F. Surface Roughness

The wind profile in the surface layer can be described as [50], [51]

$$u = \begin{cases} \dfrac{u_*}{k_a}\left(\ln\dfrac{z}{z_0} - \psi_m\right), & z/L_{\rm mo} \le 0 \\ \dfrac{u_*}{k_a}\left[\ln\dfrac{z}{z_0} - \psi_m\left(1 - \dfrac{z}{2z_i}\right)\right], & z/L_{\rm mo} \ge 0 \end{cases} \tag{29}$$

where z_i is the height of boundary layer, and ψ_m is calculated as [50]

$$\psi_m = \int_{z_0/L_{\rm mo}}^{z/L_{\rm mo}} (1-\phi_m)\,\frac{d(z/L_{\rm mo})}{z/L_{\rm mo}} \tag{30}$$

By substituting (23) into (30) and ignoring $z_0/L_{\rm mo}$, (30) can be expressed as

$$\psi_m = \begin{cases} -5z/L_{\rm mo}, & z/L_{\rm mo} > 0 \\ \ln\left\{\left[(1+x_1^2)/2\right]\left[(1+x_1)/2\right]^2\right\} \\ \quad -2\tan^{-1}x_1 + \pi/2, \\ \qquad 0 \ge z/L_{\rm mo} \ge -2 \\ (3/2)\ln\left[(x_2^2+x_2+1)/3\right] \\ \quad -\sqrt{3}\tan^{-1}\left[(2x_2+1)/\sqrt{3}\right] + \pi/\sqrt{3}, \\ \qquad z/L_{\rm mo} < -2 \end{cases} \tag{31}$$

where $x_1 = (1-16z/L_{\rm mo})^{1/4}$ and $x_2 = (1-15z/L_{\rm mo})^{1/3}$.

A smooth sea surface can be approximated as a perfectly conducting surface, and a rough sea surface can be modeled with the Miller-Brown roughness reduction factor. The wind speed at 10 m height, U_{10}, is used to represent the on-shore wind under a near-neutral atmospheric condition.

G. Evaporation Duct Height

Duct height variation with wind speed has been reported in [62]. The coastal areas are especially rich in super-refractive layers and ducts that affect microwave propagation [63]. In [64], cumulative distribution functions of duct height are derived in three locations. A larger variation in duct height is observed around the Lucinda data than in the Coral Sea. When sea breezes are the dominant wind flow, duct heights can be highly variable over a 24 hour cycle. The ducting events in the Coral Sea occurred under stable weather conditions, with little variation in wind speed; while the ducting events in the Western Pacific Ocean shows the greatest variation in duct height because of the highly variable weather.

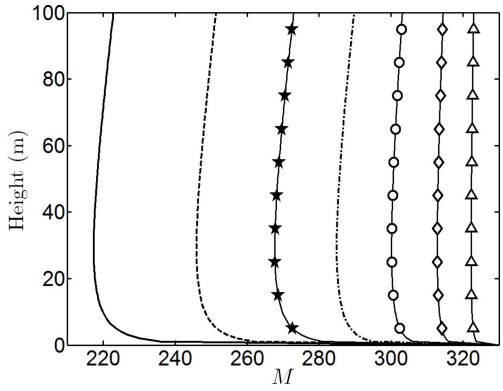

Fig. 1. Modified refractivity profiles in an evaporation duct with $M(0) = 330$, $z_d = 29$ m, ——: very unstable, − − −: unstable, — —: near-neutral unstable, −.−: neutral, —○—: near-neutral stable, —◇—: stable, —△—: very stable, $L_{\rm mo}$ and z_0 of table I are used.

IV. Simulation and Discussions

Fig.1 shows examples of modified refractivity profiles expressed in (16), in an evaporation duct with $z_d = 29$ m, under seven atmospheric conditions as listed in Table I.

The difference of M values at the duct height and on the sea surface changes significantly under different atmospheric conditions. The atmospheric condition is well correlated to the Monin-Obukhov length, $L_{\rm mo}$, and the latter can be estimated using the Richardson number, R_i, as in (17). The Richardson number is a function of the Bowen ratio, as in (18), and the latter is expressed in (19). When the atmosphere becomes more unstable, the humidity gradient, $\partial q/\partial z$, increases in magnitude, leading to a stronger duct, or a larger difference of M values at the duct height and on the sea surface.

A one-dimensional (vertical) Kolmogorov spectrum is adopted in [23], hence the phase fluctuation of waves propagating in the horizonal direction is not considered. This approximation is reasonable if the step size, Δx, in the SSF model is much larger than L_{0h}. However, when the atmosphere becomes more unstable, the horizontal outer scale increases and may become comparable to Δx [55]. In that case, a two-dimensional spectrum is more suitable.

In this work, the two-dimensional anisotropic Kolmogorov spectrum of refractive-index fluctuation in (15) is adopted, with the outer scale of the turbulence in the surface layer expressed in (24), the structure constant in an evaporation duct expressed in (28), and the L_{0h}/L_{0v} ratio under $z/L_{\rm mo} < 0.5$ expressed in (26).

Figs.2, 3 and 4 show the variations of the vertical outer scale, L_{0v}, the structure constant, C_n^2, and the L_{0h}/L_{0v} ratio, respectively, covering all the seven atmospheric conditions listed in Table I. Since evaporation ducts are formed only tens of meters above the sea surface, the meteorological models which are valid in the surface layer are sufficient to characterize these ducts.

The outer scales under unstable conditions are much larger than those under stable conditions, which has been confirmed by observations [55]. Under unstable conditions, the outer scale grows with height, as the air convection tends to reduce the wind shear. Under stable conditions, the outer scale tends

to decrease with height, as the stratification process tends to increase the wind shear. Accompanied by larger refractive-index fluctuation and larger outer scales, the structure constant under unstable conditions becomes much larger than that under stable conditions. Fig.1 implies that, under unstable conditions, stronger ducting effect allows the wave to propagate with a larger grazing angle, which in turns suffers stronger scattering effect by the rough sea surface [19]. Figs.2 and 3 indicate that, under unstable conditions, C_n^2 and L_0 become larger, hence the air turbulence gets stronger. The surface layer usually appears in the lowest 10 % of the boundary layer. At the height above $z_i/10$, the height profiles of C_n^2, L_{0v} and L_{0h}/L_{0v}, as shown in Figs.1, 2, 3 and 4, respectively, may not be accurate enough. Since the propagation properties in and near the surface layer are of major concern, less accurate profiles at higher altitudes should cause little problem.

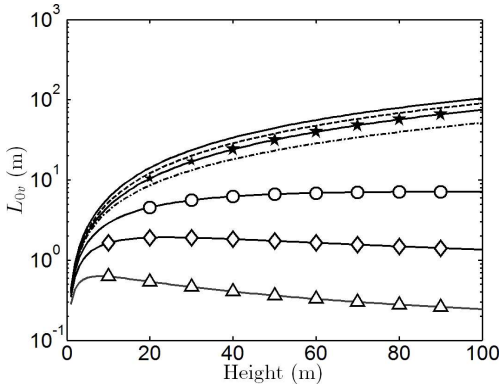

Fig. 2. Vertical outer scale L_{0v} over height, ——: very unstable, − − −: unstable, — —: near-neutral unstable, −.−: neutral, —○—: near-neutral stable, —◇—: stable, —△—: very stable, $L_{\rm mo}$ of table I is used.

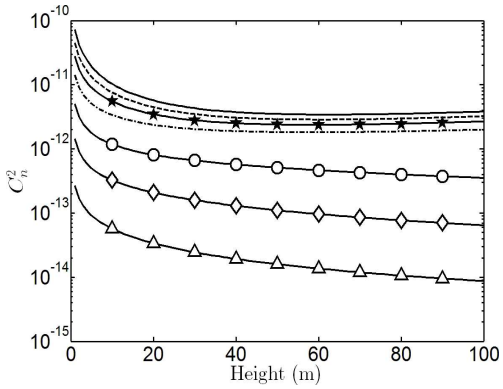

Fig. 3. Structure constant C_n^2 over height, ——: very unstable, − − −: unstable, — —: near-neutral unstable, −.−: neutral, —○—: near-neutral stable, —◇—: stable, —△—: very stable, $L_{\rm mo}$ and z_0 of table I are used.

As shown in Fig.4, the L_{0h}/L_{0v} ratio in a very stable air ($z/L_{\rm mo} \geq 0.5$) becomes unpredictable when $z \geq 0.5L_{\rm mo}$, yet its average value above $0.5L_{\rm mo}$ is close to those in a slightly unstable air [50], [58]. In this work, the L_{0h}/L_{0v} ratio in $z \geq 0.5L_{\rm mo}$ is approximated as that of a neutral air, namely, $L_{0h}/L_{0v} = 1.592$. The reference wind speed at 10 m above the sea is estimated with (29).

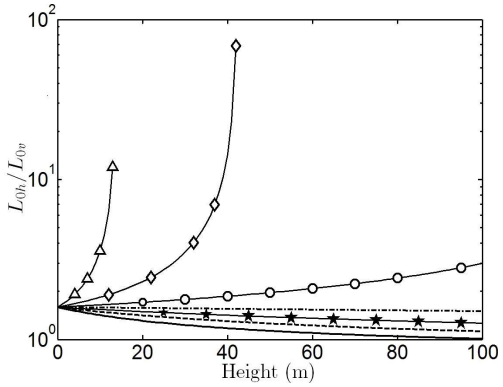

Fig. 4. Anisotropy ratio L_{0h}/L_{0v} over height, ——: very unstable, − − −: unstable, — —: near-neutral unstable, −.−: neutral, —○—: near-neutral stable, —◇—: stable, —△—: very stable, $L_{\rm mo}$ of table I is used.

Referring to [65], we choose $z_d = 29$ m, $z_t = 4$ m, $f = 10.6$ GHz, in the subsequent simulations. The wave of horizontal polarization, which is more significantly affected than the vertical polarization in the two-dimensional case, is chosen. Radio signals in the 10.6 GHz band are often trapped in an evaporation duct above the sea surface, hence can be transmitted well beyond the horizon. The duct height of $z_d = 29$ m is a typical number observed in the afternoon.

Figs.5 to 8 show the path-loss over range and height in evaporation ducts under very unstable (vu), neutral (n), near-neutral stable (ns), and stable (s) atmospheric conditions, respectively, as listed in Table I. The frequency is $f = 10.6$ GHz, the duct height is $z_d = 29$ m, and the transmitter antenna height is $z_t = 4$ m.

As shown in Fig.1, when the atmospheric condition progresses from stable to very unstable, the slope, $|dM/dz|$, within the duct increases significantly; and the slope outside the duct increases slightly. By comparing case (a) in Figs.5 to 8, different characteristics in the path-loss distribution is observed between the unstable ($L_{\rm mo} < 0$) and the stable ($L_{\rm mo} > 0$) conditions. Although ducts appear under all atmospheric conditions, the contrast of path-loss within the duct and outside the duct is more obvious under unstable conditions.

The path-loss distribution within the duct displays an interference pattern between the propagating wave and the reflected wave from the smooth sea surface. The period of interference pattern within the duct under very unstable condition is shorter than those under the other three conditions, which is attributed to the larger grazing angle under the former condition. The interference pattern seems to undermine the ducting effect. Under unstable condictions, the effect of rough sea surface increases as the grazing angle, χ, in (9), is increased. Meanwhile, the turbulence effect is increased as $(\partial\langle n\rangle/\partial z)^2$ in (27) is increased.

When the atmospheric condition is close to neutral ($R_i \sim 0$), (18) implies that the wind shear, $|\partial v_h/\partial z|$, becomes larger, hence the wind speed, U_{10}, also becomes higher. Note that in (8) and (9), the effect of rough sea surface is dominated by the grazing angle, χ, and the wind speed, U_{10}.

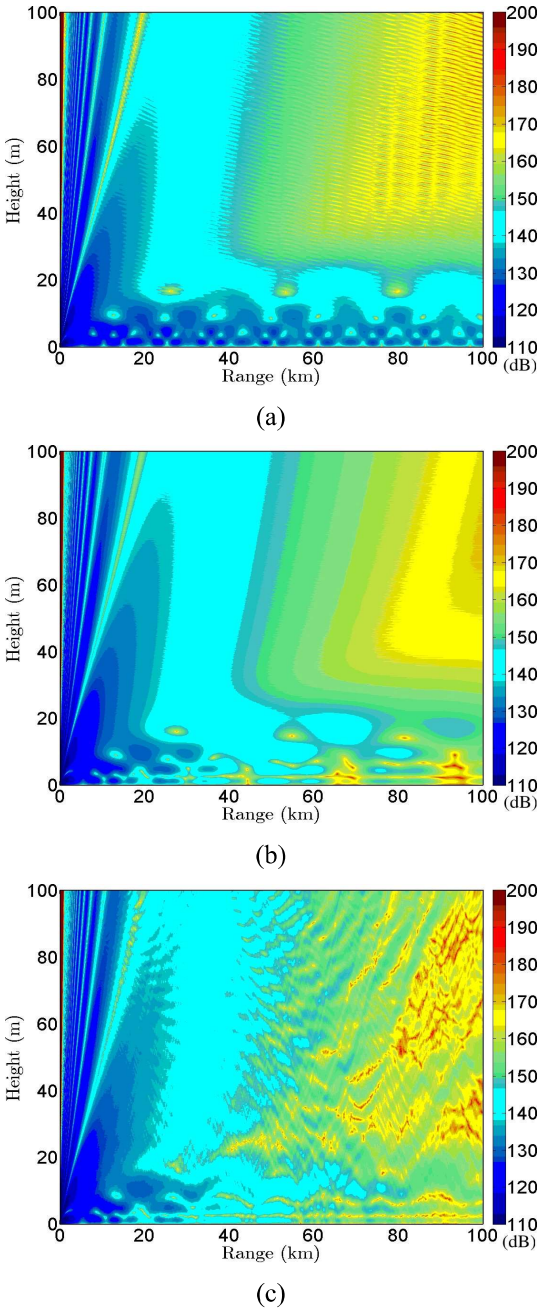

Fig. 5. Path-loss over range and height in a very unstable evaporation duct above rough sea surface, with $z_t = 4$ m, $z_d = 29$ m, $f = 10.6$ GHz, $L_{\rm mo} = -73$ m, $u_* = 0.22$ m/s, $z_0 = 6.2 \times 10^{-5}$ m, and $U_{10} = 6.4$ m/s, (a) smooth sea surface, without turbulence, (b) rough sea surface, without turbulence, (c) rough sea surface, with turbulence.

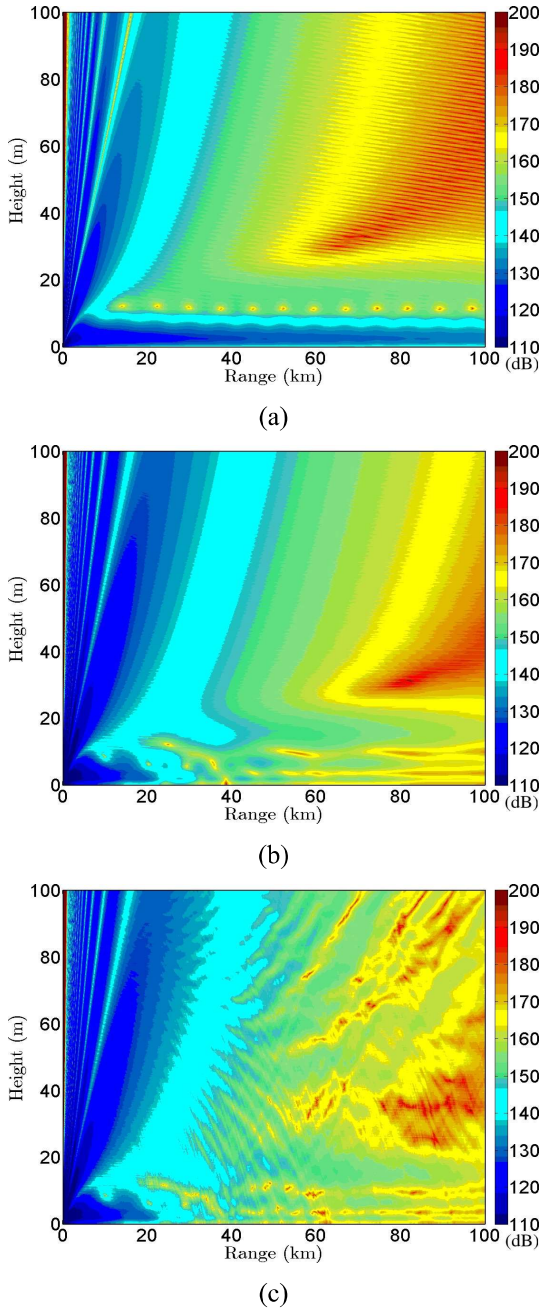

Fig. 6. Path-loss over range and height in a neutral evaporation duct above rough sea surface, with $z_t = 4$ m, $z_d = 29$ m, $f = 10.6$ GHz, $L_{\rm mo} = -1531$ m, $u_* = 0.4$ m/s, $z_0 = 19.6 \times 10^{-5}$ m, and $U_{10} = 10.81$ m/s, (a) smooth sea surface, without turbulence, (b) rough sea surface, without turbulence, (c) rough sea surface, with turbulence.

By comparing case (b) and case (a) in Figs.5 to 8, the path-loss near the sea surface at long ranges in case (b) (with rough sea surface) is always larger than that in the corresponding case (a) (with smooth sea surface). On the other hand, the path-loss at the same range but higher altitudes in case (b) becomes smaller than its counterpart in case (a). This phenomenon of energy leakage (from the duct to the air above) may be attributed to the scattering by the rough sea surface. The leakage phenomenon is more obvious under very unstable and neutral conditions.

Eqns.(8) and (9) suggest that the roughness effect of sea surface becomes more obvious as the grazing angle increases and/or the wind speed increases. As shown in Fig.1, a larger gradient of refractive index is observed near the sea surface when the atmosphere is more unstable, causing a larger grazing angle. Based on (29), the wind speed, U_{10}, becomes larger when the atmospheric condition is close to neutral.

The path-loss distributions under unstable (u) and near-neutral unstable (nu) conditions appear similar to those under very unstable (vu) condition and neutral (n) condition,

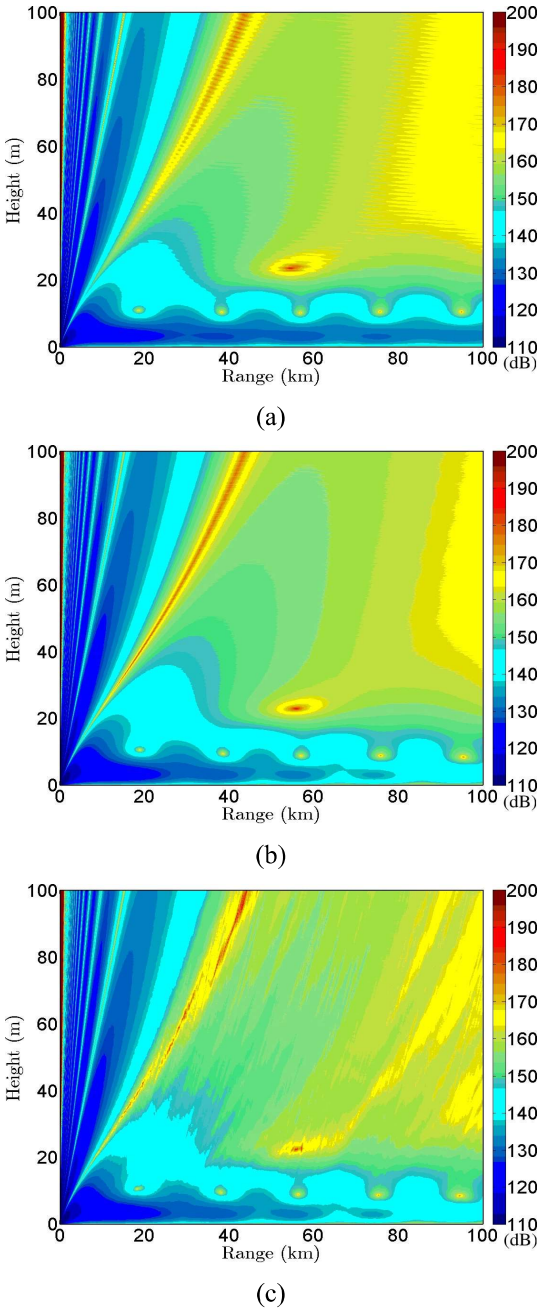

Fig. 7. Path-loss over range and height in a near-neutral stable evaporation duct above rough sea surface, with $z_t = 4$ m, $z_d = 29$ m, $f = 10.6$ GHz, $L_{\rm mo} = 314$ m, $u_* = 0.23$ m/s, $z_0 = 6.3 \times 10^{-5}$ m, and $U_{10} = 6.98$ m/s, (a) smooth sea surface, without turbulence, (b) rough sea surface, without turbulence, (c) rough sea surface, with turbulence.

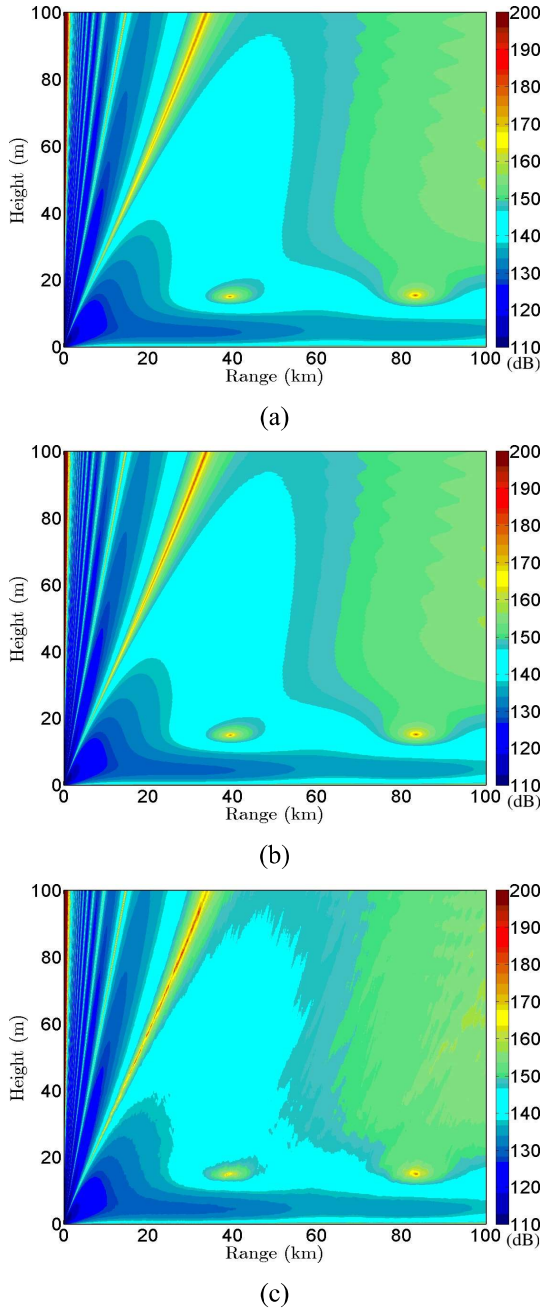

Fig. 8. Path-loss over range and height in a stable evaporation duct above rough sea surface, with $z_t = 4$ m, $z_d = 29$ m, $f = 10.6$ GHz, $L_{\rm mo} = 85$ m, $u_* = 0.15$ m/s, $z_0 = 2.9 \times 10^{-5}$ m, and $U_{10} = 5$ m/s, (a) smooth sea surface, without turbulence, (b) rough sea surface, without turbulence, (c) rough sea surface, with turbulence.

respectively, hence are not presented. Under very stable (vs) condition, neither the rough sea surface nor the air turbulence generates noticeable difference in the path-loss. Hence, it is not presented, either.

As shown in Fig.3, the structure constant decreases with height. This tendency is predictable from (27), using the profiles of $|dM/dz|$ and L_{0v} shown in Figs.1 and 2, respectively. Larger value of C_n^2 implies stronger turbulence intensity, especially under neutral and unstable conditions. Although larger value of C_n^2 is observed near the sea surface, under all conditions; the turbulence effect appears more obvious at higher altitudes attributed to the outer scales in the Kolmogorov spectrum of (15). As the atmospheric condition progresses from neutral to very unstable, the turbulence creates strong interference in the upper right quarter of the path-loss distribution, and significantly increases the path-loss in that area. The path-loss in the duct is increased by the order of 10 dB at the range of 100 km.

Fig.9 shows the standard deviation of path-loss below the duct height of $z_d = 29$ m, based on the data presented in Figs.5

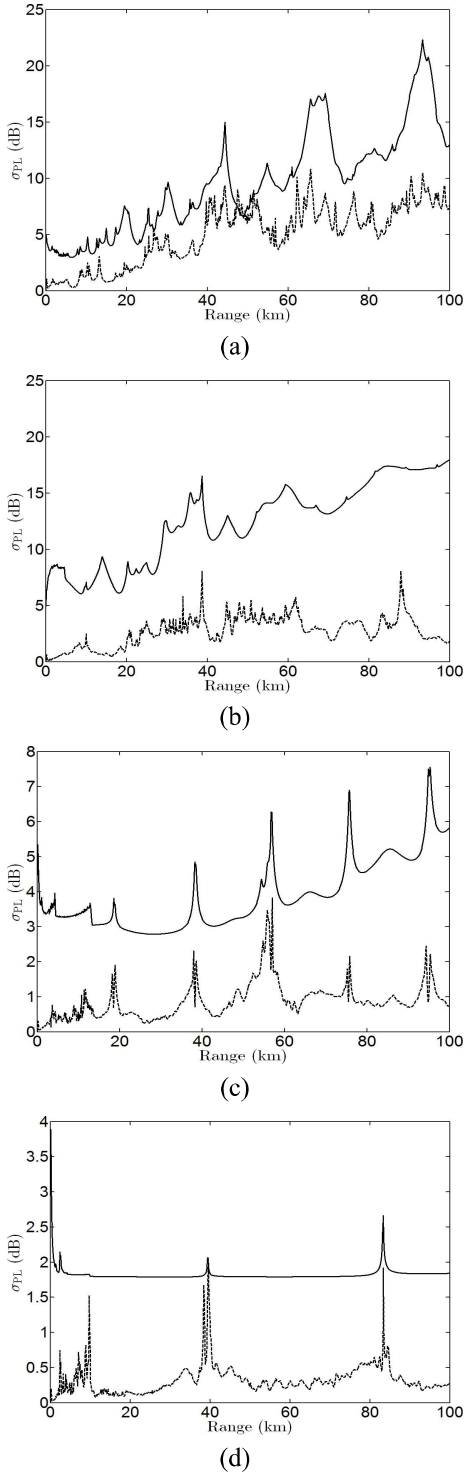

Fig. 9. Standard deviation of path-loss within the duct ($z_d = 29$ m), ——: effect of rough sea surface, — — —: effect of turbulence, (a) very unstable condition (vu), (b) neutral condition (n), (c) near-neutral stable condition (ns), (d) stable condition (s).

to 8. The standard deviation of path-loss, at a given range, attributed to the rough sea surface is derived by taking the root-mean-square (rms) difference between the data with smooth sea surface (case (a)) and those with rough sea surface (case (b)). Similarly, the standard deviation of path-loss, at a given range, attributed to the turbulence is derived by taking the root-mean-square difference between the data with rough sea surface without turbulence (case (b)) and those with turbulence (case (c)).

Strong rough sea surface effect is observed under very unstable and neutral conditions, attributed to the strong ducting effect under very unstable condition, as shown in Fig.1, and the high wind speed under neutral condition, in (17) and (18). The rough sea surface contributes no obvious effect under near-neutral stable and stable conditions, due to the low wind speed and weak ducting. As the atmospheric condition progresses from stable to very unstable, additional path-loss due to turbulence gradually increases, as can be predicted from Figs.2 and 3.

The main contribution of this work is to simulate the combined effects of rough surface and inhomogeneous atmosphere to the propagation in evaporation ducts. Although many experimental works have been successfully conducted before, it still requires some theoretical analysis and simulation to differentiate the separate effects of the aforementioned mechanisms. The parameters chosen in this work are closely tied to the previous experiments, hence the simulation results are complementary to those works. A two-dimensional simulation scenario takes less computational burden to study these effects. The simulation approach in this work can be extended to three-dimensional cases (with two-dimensional rough surfaces), only at a heavier computational load.

The paraxial approximation leads to more accurate predictions at high frequencies and in the forward direction. In this work, the frequency is chosen to be 10.6 GHz, and the propagation direction in evaporation ducts is pretty much forward. When using the split-step Fourier method, the step size in the propagation direction is restricted by the minimum scale length of the inhomogeneous atmosphere. The step size becomes very small if the tiny details of the atmosphere is to be included, then the computational time will be increased and numerical instability may occur at long distances.

V. Conclusion

A proper set of physical and mathematical models have been compiled to analyze and simulate wave propagation in evaporation ducts, under the scattering effect of rough sea surface and the air turbulence. All the relevant parameters are clearly connected to seven possible atmospheric conditions. A systematic approach, including the range of parameters, has been proposed to simulate wave propagation in close-to-realistic evaporation ducts. Simulations have also been conducted to demonstrate the effectiveness of this model and approach.

The split-step Fourier propagation algorithm has been applied to analyze the propagation properties in evaporation ducts above a rough sea surface, incorporating the turbulence effect. The PJ model of modified refractivity under different atmospheric conditions is adopted in our model, which renders significant difference of path-loss distribution under different atmospheric conditions.

The scattering effect of the rough sea surface is simulated by introducing a correction factor of surface roughness into the

boundary condition. When the atmosphere is more unstable, the interference pattern within a duct bears a shorter period and a wider range of path-loss variation.

The turbulence is described with a two-dimensional Kolmogorov spectrum, in which the structure constant of refractive index fluctuation, the outer scales of turbulence, and the anisotropy of the outer scales are well connected to different atmospheric conditions.

Significant effects of rough sea surface and air turbulence are observed under neutral ($|L_{\rm mo}| \sim \infty$) and unstable ($L_{\rm mo} < 0$) conditions. The effect of rough sea surface is less significant under stable ($L_{\rm mo} > 0$) conditions, accompanied by low grazing angle and low wind speed. The effect of air turbulence gradually increases as the atmospheric condition progresses from stable to unstable, accompanied by larger eddy size and stronger turbulence intensity.

REFERENCES

[1] A. V. Kukushkin, V. D. Freilikher, and I. M. Fuks, "Transhorizon propagation of ultrashort radio waves above the sea (review)," *Radiofizika*, vol.30, no.7, pp.811-839, 1987.

[2] K. V. Koshel and A. A. Shishkarev, "Influence of layer and anisotropic fluctuations of the refractive index on the beyond-the-horizon SHF propagation in the troposphere over the sea when there is an evaporation duct," *Waves in Random Media*, vol.3, no.1, pp.25-38, 1993.

[3] F. T. Ulaby, R. K. Moore, and A. K. Fung, "Microwave remote sensing fundamentals and radiometry," in *Microwave Remote Sensing: Active and Passive*, vol. 1, Addison-Wesley, 1981.

[4] F. Mesnard and H. Sauvageot, "Climatology of anomalous propagation radar echoes in a coastal area," *J. Appl. Meteorol. Climatol.*, vol.49, no.11, pp. 2285-2300, 2010.

[5] M. I. Skolnik, *Introduction to Radar Systems*, 3rd ed., McGraw-Hill, 2001.

[6] R. Douvenot, V. Fabbro, P. Gerstoft, C. Bourlier, and J. Saillard, "A duct mapping method using least squares support vector machines," *Radio Sci.*, vol.43, pp.1-12, 2008.

[7] K. D. Anderson, "Radar measurements at 16.5 GHz in the oceanic evaporation duct," *IEEE Trans. Antennas Propagat.*, vol.37, no.1, pp.100-106, 1989.

[8] B. W. Atkinson, J-G. Li, and R. S. Plant, "Numerical modeling of the propagation environment in the atmospheric boundary layer over the Persian Gulf," *J. Appl. Meteorol. Climatol.*, vol.40, no.3, pp.586-603, 2001.

[9] A. Kerans, A. S. Kulessa, E. Lensson, G. French, and G. S. Woods, "Implications of the evaporation duct for microwave radio path design over tropical oceans in Northern Australia," *Workshop Appl. Radio Sci.*, Leura, Australia, 2002.

[10] I. Sirkova and M. Mikhalev, "Parabolic-equation-based study of ducting effects on microwave propagation," *Microwave Opt. Technol. Lett.*, vol.42, no.5, pp.390-394, 2004.

[11] I. Sirkova and M. Mikhalev, "Influence of tropospheric ducting on microwave propagation in short distances," *EURO-COST 273 TD(02) 086*, Espoo, Finland, 2002.

[12] I. Sirkova and M. Mikhalev, "Influence of tropospheric duct parameters changes on microwave path loss," *Proc. Int. Sci. Conf. Inf. Commun. Energy Syst. Technol.*, Sofia, Bulgaria, pp.43-46, 2003.

[13] S. S. Mentes and Z. Kaymaz, "Investigation of surface duct conditions over Istanbul, Turkey," *J. Appl. Meteorol. Climatol.*, vol.46, no.3, pp.318-337, 2007.

[14] I. Sirkova, "Path loss calculation for a surface duct statistics," *Proc. Int. Sci. Conf. Inf. Commun. Energy Syst. Technol.*, Veliko Tarnovo, Bulgaria, pp.53-56, 2009.

[15] H. Hitney and R. Vieth, "Statistical assessment of evaporation duct propagation," *IEEE Trans. Antennas Propagat.*, vol.38, no.6, pp.794-799, 1990.

[16] H. V. Hitney and L. R. Hitney, "Frequency diversity effects of evaporation duct propagation," *IEEE Trans. Antennas Propagat.*, vol.38, no.10, pp.1694-1700, 1990.

[17] R. A. Paulus, "Practical application of an evaporation duct model," *Radio Sci.*, vol.20, no.4, pp.887-896, 1985.

[18] A. Kukushkin and J. Wiley, *Radio Wave Propagation in the Marine Boundary Layer*, Wiley Online Library, 2004.

[19] H. V. Hitney, "Evaporation duct propagation and near-grazing angle scattering from a rough sea," *IEEE Int. Geosci. Remote Sensing Symp.*, pp.2631-2633, 1999.

[20] D. Rouseff, "Simulated microwave propagation through tropospheric turbulence," *IEEE Trans. Antennas Propagat.*, vol.40, no.9, pp.1076-1083, 1992.

[21] H. V. Hitney, "A practical tropospheric scatter model using the parabolic equation," *IEEE Trans. Antennas Propagat.*, vol.41, no.7, pp.905-909, 1993.

[22] A. Barrios, "Modeling surface layer turbulence effects at microwave frequencies," *IEEE Radar Conf.*, 2008.

[23] I. Levadnyi, V. Ivanov, and V. Shalyapin, "Simulation of microwave propagation in turbulent evaporation duct," *Euro, Conf. Antennas Propagat.*, 2012.

[24] M. Levy, *Parabolic Equation Methods for Electromagnetic Wave Propagation*, Inst. Electr. Eng., 2000.

[25] O. Benhmammouch, N. Caouren, and A. Khenchaf, "Influence of sea surface roughness on electromagnetic waves propagation in presence of evaporation duct," *Int. Radar Conf.*, 2009.

[26] T. S. Hristov, K. D. Anderson, and C. A. Friehe, "Scattering properties of the ocean surface: the Miller-Brown-Vegh model revisited," *IEEE Trans. Antennas Propagat.*, vol.56, no.4, pp.1103-1109, 2008.

[27] Y. V. Levadnyi, V. K. Ivanov, and V. N. Shalyapin, "Simulation of microwave propagation in evaporation duct over rough sea surface (in Russian)," *Radiophys. Electron.*, vol.14, pp.28-34, 2004.

[28] J. R. Kuttler and G. D. Dockery, "Theoretical description of the parabolic approximation/Fourier split-step method of representing electromagnetic propagation in the troposphere," *Radio Sci.*, vol.26, no.2, pp.381-393, 1991.

[29] G. Apaydin and L. Sevgi, "FEM-based surface wave multimixed-path propagator and path loss predictions," *IEEE Antennas Wireless Propagat. Lett.*, vol.8, pp.1010-1013, 2009.

[30] A. S. Kulessa, G. S. Woods, B. Piper, and M. L. Heron, "Line-of-sight EM propagation experiment at 10.25 GHz in the tropical ocean evaporation duct," *IEE Proc. Microwaves Antennas Propagat.*, vol.145, no.1, pp.65-69, 1998.

[31] H. Essen and H. H. Fuchs, "Microwave and millimeterwave propagation within the marine boundary layer," *German Microwave Conf.*, Karlsruhe, Germany, 2006.

[32] S. D. Gunashekar, E. M. Warrington, D. R. Siddle, and P. Valtr, "Signal strength variations at 2 GHz for three sea paths in the British channel islands: Detailed discussion and propagation modeling," *Radio Sci.*, vol.42, no.4, pp.1-13, 2007.

[33] V. K. Ivanov, V. N. Shalyapin, and Y. V. Levadny, "Microwave scattering by tropospheric fluctuations in an evaporation duct," *Radiophys. Quantum Electron.*, vol.52, no.4, pp.277-286, 2009.

[34] G. Bein, "Monte Carlo computer technique for one-dimensional random media," *IEEE Trans. Antennas Propagat.*, vol.21, no.1, pp.83-88, 1973.

[35] R. N. Adams and E. D. Denman, *Wave Propagation and Turbulent Media*, Elsevier, 1966.

[36] G. L. Geernaert, "On the evaporation duct for inhomogeneous conditions in coastal regions," *J. Appl. Meteorol. Climatol.*, vol.46, no.4, pp.538-543, 2007.

[37] S. A. Raid, J. Z. Gehman, J. R. Kuttler, and M. H. Newkirk, "Modeling radar propagation in three-dimensional environments," *Johns Hopkins APL Tech. Digest*, vol.25, no.2, p.101, 2004.

[38] R. Janaswamy, "Path loss predictions in the presence of buildings on flat terrain: A 3-D vector parabolic equation approach," *IEEE Trans. Antennas Propagat.*, vol.51, no.8, pp.1716-1728, 2003.

[39] J. P. Zhang, Z. S. Wu, Q. L. Zhu, and B. Wang, "A four-parameter m-profile model for the evaporation duct estimation from radar clutter," *Prog. Electromag. Res.*, vol.114, pp.353-368, 2011.

[40] G. D. Dockery, R. Awadallah, D. E. Freund, J. Z. Gehman, and M. H. Newkirk, "An overview of recent advances for the TEMPER radar propagation model," *IEEE Radar Conf.*, pp.896-905, 2007.

[41] R. Frehlich, "Simulation of laser propagation in a turbulent atmosphere," *Appl. Opt.*, vol.39, no.3, pp.393-397, 2000.

[42] A. R. Miller, R. M. Brown, and E. Vegh, "New derivation for the rough-surface reflection coefficient and for the distribution of sea-wave elevations," *IEE Proc. H: Microwaves Opt. Antennas*, vol.131, no.2, pp.114-116, 1984.

[43] D. Dockery and J. R. Kuttler, "An improved impedance-boundary algorithm for Fourier split-step solutions of the parabolic wave equation," *IEEE Trans. Antennas Propagat.*, vol.44, no.12, pp.1592-1599, 1996.

[44] W. L. Patterson, C. P. Hattan, H. V. Hitney, R. A. Paulus, and G. E. Lindem, "Engineer's refractive effects prediction system (EREPS) version 3.0," DTIC Doc. ADA283748, 1994.

[45] D. E. Freund, N. E. Woods, H. C. Ku, and R. S. Awadallah, "The effects of shadowing on modelling forward radar propagation over a rough sea surface," *Waves Random Complex Medium*, vol.18, pp.387-408, 2008.

[46] G. I. Taylor, "The spectrum of turbulence," *Proc. R. Soc. London, Ser. A*, vol.164, no.919, pp.476-490, 1938.

[47] A. Ishimaru, *Wave Propagation and Scattering in Random Media* , IEEE Press, 1997.

[48] N. Wiener, "Generalized harmonic analysis," *Acta Mathematica*, vol.55, no.1, pp.117-258, 1930.

[49] R. A. Paulus, "Specification for environmental measurements to assess radar sensors," DTIC Doc., 1989.

[50] H. A. Panovsky and J. A. Dutton, *Atmospheric Turbulence: Models and Methods for Engineering Applications*, John Wiley, 1984.

[51] S. E. Gryning, E. Batchvarova, B. Brümmer, H. Jørgensen, and S. Larsen, "On the extension of the wind profile over homogeneous terrain beyond the surface boundary layer," *Boundary Layer Meteorol.*, vol.124, no.2, pp.251-268, 2007.

[52] A. Peña, S. E. Gryning, and C. B. Hasager, "Measurements and modelling of the wind speed profile in the marine atmospheric boundary layer," *Boundary Layer Meteorol.*, vol.129, no.3, pp.479-495, 2008.

[53] V. I. Tatarskii, *The Effects of the Turbulent Atmosphere on Wave Propagation*, Israel Program for Scientific Translations, 1971.

[54] Z. Sorbjan, *Structure of the Atmospheric Boundary Layer*, Prentice Hall, 1989.

[55] A. Lüdi and A. Magun, "Near-horizontal line-of-sight millimeter-wave propagation measurements for the determination of outer length scales and anisotropy of turbulent refractive index fluctuations in the lower troposphere," *Radio Sci.*, vol.37, no.2, pp.12.1-19, 2002.

[56] A. Lüdi and A. Magun, "Refractivity structure constant and length scales from mm-wave propagation in the stably stratified troposphere," *J. Atmos. Sol. Terr. Phys.*, vol.67, no.5, pp.435-447, 2005.

[57] R. Soucy, R. Woodward, and H. A. Panofsky, "Vertical cross-spectra of horizontal velocity components at the Boulder observatory," *Boundary Layer Meteorol.*, vol.24, no.1, pp.57-66, 1982.

[58] A. J. Bowen, R. G. J. Flay, and H. A. Panofsky, "Vertical coherence and phase delay between wind components in strong winds below 20 m," *Boundary Layer Meteorol.*, vol.26, no.4, pp.313-324, 1983.

[59] D. C. Cox, H. W. Arnold, and H. H. Hoffman, "Observations of cloud-produced amplitude scintillation on 19-and 28-GHz Earth-space paths," *Radio Sci.*, vol.16, no.5, pp.885-907, 1981.

[60] A. Tunick, "Optical turbulence effects on ground to satellite microwave refractivity," DTIC Doc. ADA449682, 2006.

[61] S. D. Burk, "Refractive index structure parameters-time-dependent calculations using a numerical boundary-layer model," *J. Appl. Meteorol.*, vol.19, pp.562-576, 1980.

[62] A. S. Kulessa, M. L. Heron, and G. S. Woods, "Temporal variations in evaporation duct heights," *Proc. WARS'97*, pp.165-170, 1997.

[63] J. D. Turton, D. A. Bennetts, and S. F. G. Farmer, "An introduction to radio ducting," *Meteorol. Mag.*, vol.117, no.1393, pp.245-254, 1988.

[64] A. Kerans, A. S. Kulessa, E. Lensson, G. French, and G. S. Woods, "Implications of the evaporation duct for microwave radio path design over tropical oceans in Northern Australia," *Proc. WARS'02*, Leura, Australia, 2002.

[65] A. Kerans, G. S. Woods, E. Lensson, and G. French, "Propagation at 10.6 GHz over a long path in the tropical evaporation duct," *Proc. WARS'02*, Leura, Australia, 2002.

Yung-Hsiang Chou was born in Taipei, Taiwan, on March 25, 1989. He received the B.S. degree in electrical engineering from National Central University, Jhongli, Taiwan, in 2011 and the M.S. degree in communication engineering from National Taiwan University, Taipei, Taiwan, in 2013.

Jean-Fu Kiang received his Ph.D. degree in electrical engineering, from the Massachusetts Institute of Technology in 1989. He has been a professor of the Department of Electrical Engineering and the Graduate Institute of Communication Engineering, National Taiwan University since 1999. He has been interested in electromagnetic applications and system issues, including wave propagation in different environments, antennas and arrays, radar and navigation, RF and microwave systems.

Editorial Comment

In this work the authors have addressed a very challenging problem, namely that of evaluating the effect of turbulence on wave propagation in evaporation ducts above a rough surface. Several different available models have been used to simulate the problem, and the results of these simulations are presented as well as discussed.